10.24425/acs.2020.134674

Archives of Control Sciences
Volume 30(LXVI), 2020
No. 3, *pages 471–500*

Control of complex dynamic nonlinear loading process for electromagnetic mill

SZYMON OGONOWSKI, DARIUSZ BISMOR and ZBIGNIEW OGONOWSKI

Electromagnetic mill installation for dry grinding represents a complex dynamical system that requires specially designed control system. The paper presents model-based predictive control which locates closed loop poles in arbitrary places. The controller performs as gain scheduling prototype where nonlinear model – artificial recurrent neural network, is parameterized with additional measurements and serves as a basis for local linear approximation. Application of such a concept to control electromagnetic mill load allows for stable performance of the installation and assures fulfilment of the product quality as well as the optimization of the energy consumption.

Key words: predictive control, pole placement, nonlinear dynamics, neural modelling, electromagnetic mill

1. Introduction

Complex and fast dynamics processes, especially nonlinear and unstable plants are difficult to model [1] and control. Such challenges are usually created by modern industry where reduction of the cost production and increasing quality demands to impose optimization of the environment and technology. One of the main reason of such complexity are processes' recycles of material streams and energy. Persuasive examples are detailed in [2]: power generation and transmission, metal processing, marine control systems aero-engine and flight control design. In this research electromagnetic mill (EMM) serves as the example of complex production process. EMM is a novel construction which allows for fine and ultra-fine grinding. Dynamics complexity is imposed by a special construc-

All authors are with Department of Measurements and Control Systems, Faculty of Automatic Control, Electronics and Computer Science, Silesian University of Technology, Gliwice, Poland. Corresponding author is S. Ogonowski, e-mail: szymon.ogonowski@polsl.pl.

Received 12.02.2020. Revised 16.07.2020.

tion of the over-sized grains recycle and fast grinding. EMM stands out in grinding solutions thus provides interesting modelling and control problems.

Generally, grinding in various types of mills is one of the most popular processing operation used in mining, minerals, aggregates, chemical, building and food industries among others [3]. Basics of the process phenomena as well as the typical grinding circuits are well known and described in the literature [4]. The main purpose of the process is to reduce the average grain size of the processed material by smashing, breaking, attrition, pealing, cutting, crushing and other actions performed in dry or wet environment. In many applications it also serves as a preparation stage for the following processing operations. In mineral processing, grinding is a part of the processing circuit which aim is to concentrate the valuable minerals contained in raw ores. Minerals are first liberated from the ore matrix by crushing, grinding and particle size separation processes. In the next stage they are separated from the gangue using processes that selects particles based on their physical or chemical properties, such as surface hydrophobicity, specific gravity, magnetic susceptibility, chemical reactivity or color [3]. The preparation stage using grinding is thus essential for the whole concentration process effectiveness. Moreover, it is usually one of the most energy consuming stages of the whole production chain [5]. This is the main motivation for the research on the new mills' constructions, grinding and classification circuits design or optimization and effective control of the grinding process [6]. Control of the grinding process in the standard drum mill in the open circuit is usually performed as an ratio-control of the process material stream and the transport medium stream determined by the required processing time. Size reduction efficiency is, however, susceptible to the varying parameters of the feed stream (crushability, graining, moisture content) that are usually difficult to measure on-line. Other important factors concern mass and physical state of the grinding media (balls, rods, cylpebs) in the mill or the state of the working chamber liners. Usually, closed milling circuits are applied, to improve the overall efficiency of the grinding process. In such circuits the mill discharge is directed to the separation process which redirects the oversized particles to the mill input in the form of the recycle. Fine particles are directed to the following stages of the process as a grinding product. In most industries recycle flowrate is several times higher than the feed flowrate, what significantly influences the process dynamics [4]. In modern solutions that tend to limit the processing time for the energy consumption optimization purposes, grinding process dynamics are becoming even more complex and are influenced by yet another factors as grinding media rotations speed, vibration frequency, temperature and humidity of the transporting gases or electrostatic forces in the installation. These process parameters are especially influential in fine and ultra-fine grinding processes [7].

All the above aspects of control problems are focused in EMM technology which is stressed in sec. 2. In this research it is shown that the control problem of

EMM can be effectively solved by specially designed predictive controller. Model-based predictive control (MBPC) is a well-established theory since almost four decades. Earliest development as MAC [8], DMC [9], or GPC [10] laid foundation for linear predictive control and control society has created number of different linear algorithms that exploit predictive receding horizon idea in the eighties and nineties of the last centaury. However, after seminal paper [11] it became clear that only in nonlinear case predictive control may assure significantly better results than other approaches. What is more [12] showed that every linear predictive controller can be expressed in terms of linear quadratic regulator which may mean that nothing new has been brought by MBPC. Fortunately, that is not true. Number of applications and hundreds of papers proved great value of predictive control concept mainly due to robustness [13], simplicity of implementation and other advantages [14]. However, in the context of complex nonlinear dynamics, where different approaches fail, MBPC needs solving on-line i.e. in every sampling period an optimization problem what may create significant numerical difficulty. During last two decades researches have presented different proposals to reduce numerical efforts while solving optimization problem e.g. [15] or to impose suboptimal solution e.g. [16]. One of the most effective approaches has been initialized in [17] and continued e.g. in [18, 19] namely on-line linearization which means that in every sampling period updated linear model of nonlinear plant is used to calculate manipulated variable value. This idea is also used here, however the predictive controller parameters are calculated in a special way i.e. to locate closed loop poles of the linear approximation of the plant in a chosen places.

The paper is organized as follows. In sec. 2 EMM system is described as well as the measurement method of the controlled variable which is the load of the mill chamber. The structure of the EMM control system is also described in sec. 2. Identification of the controlled plant model in form of an artificial recurrent neural network is presented in sec. 3. Mathematical background of MBPC with closed-loop pole placement is delivered in sec. 4. Sec. 5 presents application of the control algorithm to EMM system to stabilize load of the mill. The paper is ended with conclusion which presents prospective works.

2. Electromagnetic mill system for ultra-fine grinding

2.1. Design of the grinding and classification circuit

Electromagnetic mill is a novel grinding device, where a rotating electromagnetic field is directly used to move ferromagnetic grinding media in the working chamber. Fig. 1 presents an exemplary D200 EMM with a working chamber diameter equal to 200 mm. The working chamber is a non-ferromagnetic tube

surrounded by six electromagnets to create electromagnetic (EM) field (Fig. 1a). The grinding medium in the form of small ferromagnetic rods fills about 10% of the working chamber volume. The shape and size of the grinding media and the mill parameters were determined by simulations using finite element analysis, to obtain the optimum effectiveness of the magnetic force. The size parameters of the rods depend on the mill diameter and the average feed and is usually of 1–3 mm of diameter and 10–15 mm of length. When the rotating electromagnetic field is inducted in the working chamber, the medium starts to move. Collisions between the rods and the processed particles cause chaotic movement inside the chamber and increase the grinding effect (Fig. 1c). The rotating EM field inducted inside the working chamber keeps the grinding media inside the chamber only for specific operating frequencies and material flowrate range, thus adequate control of these quantities is required.

(a) (b) (c)

Figure 1: Construction of electromagnetic mill: (a) electromagnets; (b) the mill with the cover and supply cabinet; (c) working chamber with the grinding media during operation

The nature of the grinding process in EMM allows for the control of shape parameters of the product grains. In the first stage of the grinding, the size reduction is performed mostly by breaking and splitting, caused by collisions with the grinding media. When the grain reaches certain size, it begins to abrade by slide on the surface of the grinding media. Such phenomena allow us to obtain sharp grain edges and irregular shapes or more cubic ones with soft edges. Parameters of the grinding process in EMM also influence the reactivity level and other physical properties of the product grains. Thus, EMM becomes significantly competitive to other milling solutions. Literature reports several examples of the electromagnetic mill applications [20], where the working chamber is in a fixed leaning position. Similar solutions were tested at the early stage of the research, however, the main disadvantage of such solution is foremost the strongly constrained controllability of the sliding speed and, in turn, uncontrolled grinding time. A fixed position also limits throughput control. There are applications with an adjusted angle of the chamber, but still the gravity and the friction determines the functionality of such feeding system. The above limitations forced a research

on the dedicated grinding and classification circuit for EMM. Such circuit was designed, patented [21] and tested and the idea of the circuit is presented in Fig. 2a. It assumes vertical positioning of the working chamber and feed supply from the top of the chamber. Fig. 2b presents one of the semi-industrial circuits build for the D200 EMM. Fig. 3 presents the 3D model of the installation for better illustration of the particular stream flows in the system. The following description uses labels shown in Fig. 3.

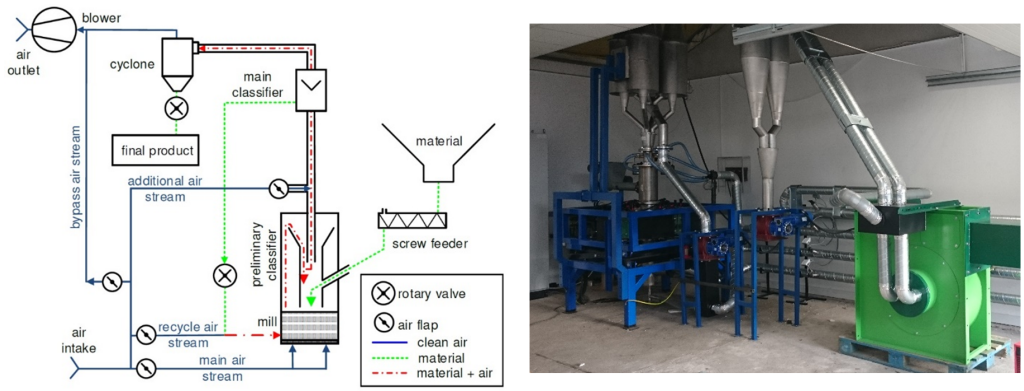

Figure 2: Dry grinding and classification circuit: (a) Circuit structure with key machines and actuators; (b) Exemplary installation with the D200 electromagnetic mill (EMM)

Material is fed to the installation by the screw feeder (no. 16) into the preliminary classifier (no. 14) situated above the mill from where larger grains drop down into the working chamber (no. 15) surrounded by 6 electromagnets which generate rotating magnetic field. Material is transported by the pneumatic transporting system. The air stream is taken form intake (no. 4) and exhausted trough the outlet (no. 3) directly connected to the main fan. The main air stream (no. 8) supplies the working chamber from the bottom and swept grinded grains up though to the preliminary classifier (where heavier part is again shifted back into the working chamber) to the main classifier (no. 13) which is parameterized by additional air stream (no. 6). The main classifier is composed of four elements working in parallel. Coarse grains leave the main classifier through the pipe (no. 12) and rotary valve (no. 2) which separates pressure to meet recycle air stream (no. 7) and to be taken back to the working chamber form its bottom side. Fine grains leave the main classifier through its top collector and are pneumatically transported to the cyclone (no. 1) which is composed with two elements working parallel. The product is collected in the bottom part of the cyclone and transported down to the tank by the rotary valve (no. 2) to separate pressure. The recovered air stream is drawn from the cyclone top by the main fan to the collector to which bypass air stream (no. 5) is also attached to reduce

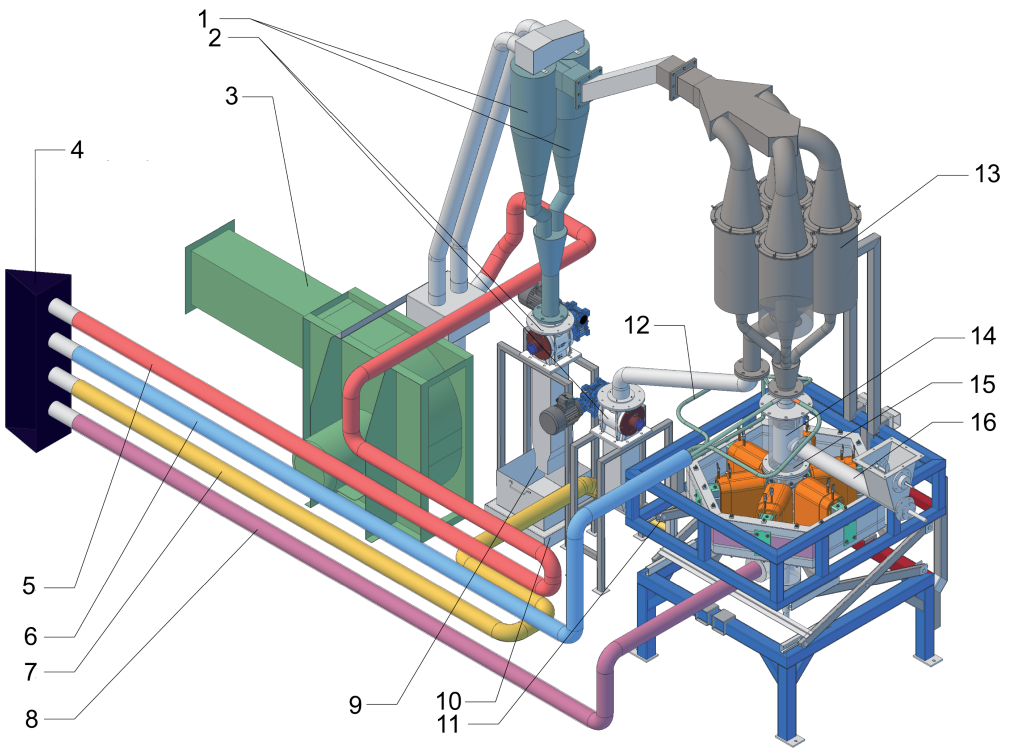

Figure 3: 3D model of the dry grinding and classification circuit with D200 EMM by ELTRAF

the total air flowrate through the working chamber and classifier. The designed circuit was intensively tested in various experiments in open and closed structures (recycle-wise) for chosen set of materials. Modelling of the air transport paths was carefully studied [22], classification capabilities were examined [23], and the control system assumptions were discussed [24]. The main conclusion from the past research is that the complex dynamics following from the structure of the novel dry grinding circuit with EMM requires specific approaches for the control of the mill load. Moreover, several key states of the system are difficult to measure or estimate, so dedicated indirect measurements needs to be applied.

2.2. Indirect measurement of the mill's load level

Measurements in mineral processing plants are always difficult to perform and usually very expensive. Solutions avoiding the measurement device contact with the processed material are preferred due to highly destructive properties of the processed material (e.g. highly abrasive grains surface). This implies indirect

measurements and soft sensing techniques applications in the systems [25, 26]. One of the most challenging task for the measurement system is the mill load determination. In the case of open circuit structure (with external recycle closed) measurement of the feed mass flowrate is sufficient and feed-forward control can be applied. When the material recycle is open, the coarse particles from the mill's output are directed to the mill again as a recycle stream. Since the measurement of the recycle mass flowrate with pneumatic conveying are difficult to conduct the problem becomes more complex. Moreover, the recycle stream is inserted below the working chamber, so estimating the mill load based on fresh feed and recycle flowrates becomes even more difficult. All of the above focused the research on the load estimation based on the condition of the working chamber with grinding media and processed material inside. Because of the extremely harsh and destructive environment in the working chamber itself, no direct measurements could be applied. During research in that area several ideas were tested, including active power of the EM field inductor or transport air pressure changes measurements among others. Finally, indirect measurement based on acoustic signal generated by the working chamber was applied [27]. A measurement microphone with cardioid polar pattern is installed on the top of the mill's working chamber on the opposite side to the fresh feed inlet (see Fig. 4a). The line gain is tuned automatically during empty mill runoff. Dedicated tuning algorithm uses information about the mill frequency and the mass of the grinding media in the working chamber [28]. Idea of the measurement is based on the observed changes in the frequency characteristics of the acoustic signal generated by the working chamber. The frequency range of the noise generated by

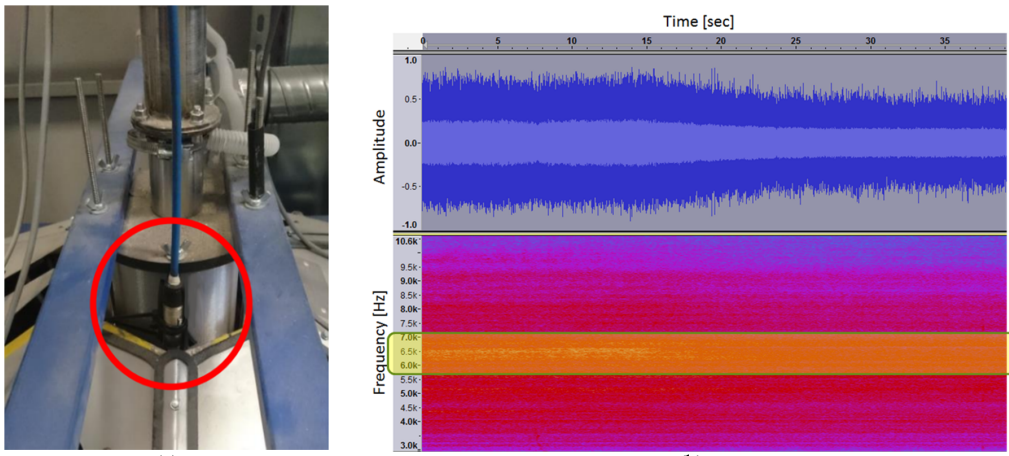

(a) (b)

Figure 4: Position of the measurement microphone (a) and time series and spectrogram of exemplary working chamber acoustic signal measurement (b)

the vibration of the EM filed inductor packages is narrow and directly proportional to the output of the frequency inverter (operating frequency of the EMM). At the same time one can observe changes in the frequency spectrum of the noise generated by the friction between rotating grinding media, walls of the working chamber and processed material. Such changes can be well observed on Fig. 4b, representing exemplary acoustic signal data. In the presented experiment working chamber of the mill was filled with grinding media and the constant output frequency was applied in the mill inverter. The mill was then successfully filled with the fresh feed starting from the 15th second of the experiment. One can notice the difference in the acoustic signal amplitude and also in the signal spectrogram in the frequency range of 6.2–6.6 kHz. The research showed that while the amplitude in time series is highly disturbed by the other circuit operating parameters changes, the spectrogram in discussed frequency range depends mostly on the mill load and operating frequency.

According to the Parseval theorem interpretation [29] total acoustic signal energy during the experiment time is equal to the sum of the energies of the frequency components in amplitude spectra in the whole range of frequencies f. For the discrete signals one can denote

$$\sum_{i=0}^{N-1} |x(i)|^2 = \frac{1}{N} \sum_{j=0}^{N-1} |X(j)|^2 \tag{1}$$

where: $X(j)$ is the amplitude spectra value for the discrete signal $x(i)$. Assuming that the average signal value equals to zero (after removing constant component) such discrete integral of the amplitude spectra is equal to the signal variance estimate. When the above is performed on the limited frequencies range the result is the signal variance in the given frequencies range. Such algorithm is applied to the working chamber acoustic signal for the specific frequency range. This specific frequency range varies naturally depending on the mill size, type of the processed material or the grinding environment (dry or wet grinding). Since the above parameters are constant for each specific application, calibration of such measurement is straightforward and can be performed based on measurement for several operating points with different load level. Fig. 5 presents values of the calibrated load level signal measured during several experiments on different types of EMM (D100 and D200), for different processed material, in dry and wet grinding. The signal was calibrated to the range of 0 to 10 to meet the industrial standard 0–10 V.

As Fig. 6 indicates, one can easily distinguish unique ranges in the measurement signal LI representing normal conditions, operation under full load and over-loaded mill operation. The ranges are disjunctive for the working frequency range of the mill's inverter form 50 Hz to 80 Hz.

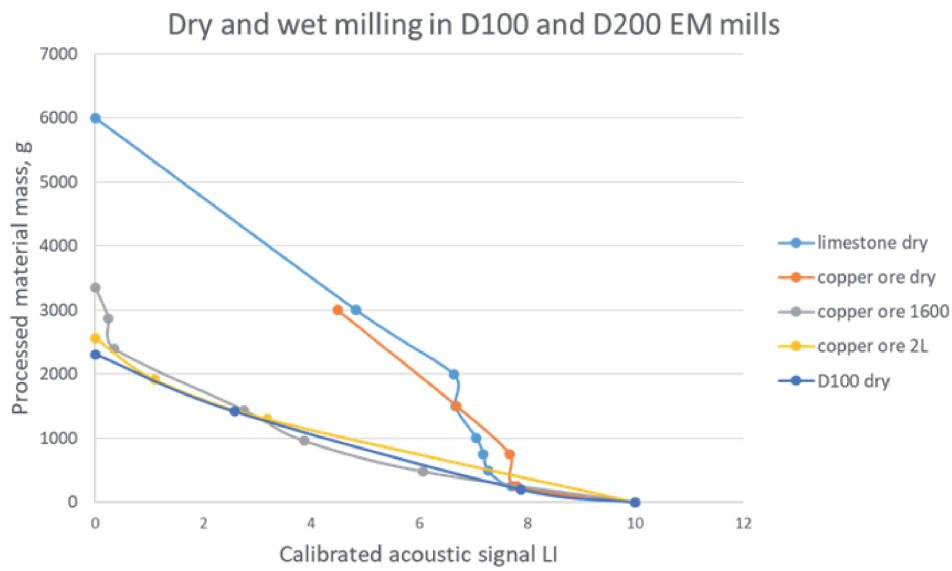

Figure 5: Exemplary measurement of mill load data for different milling conditions

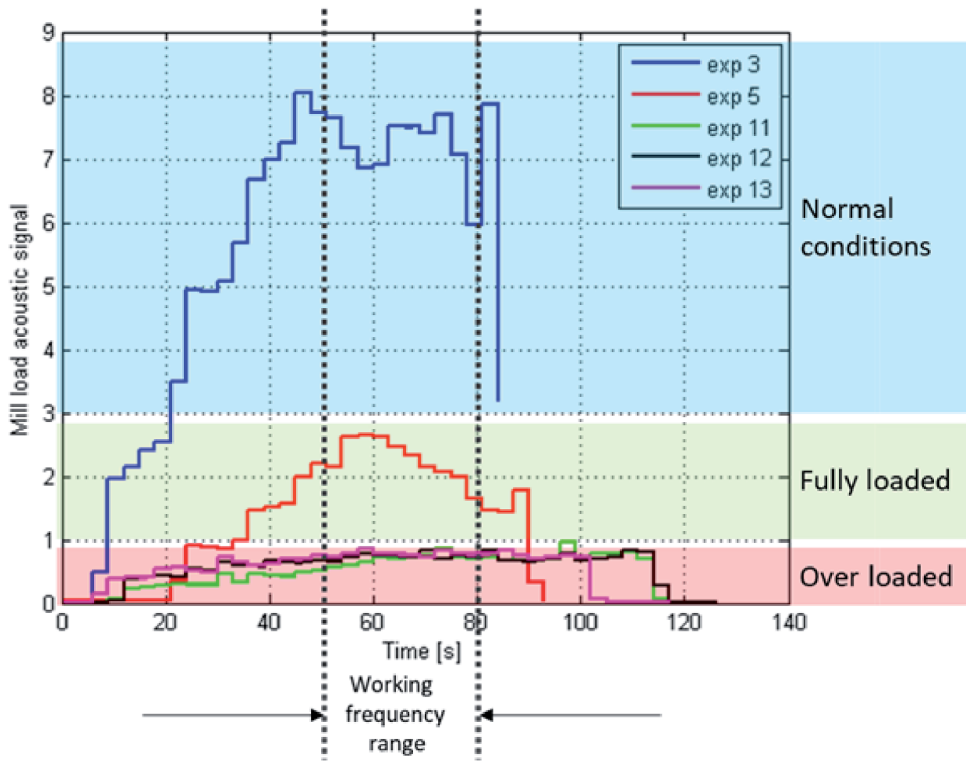

Figure 6: Mill load measurement for different operating frequency and different operating load

2.3. Structure of the load level control system

EMM installation comprises a plant to be controlled with many control goals defined for each subsystem. The most important are the parameters of the product such as grain size, shape, physical, and chemical properties. To meet these requirements, every subsystem in the installation needs to perform properly in the nominal conditions, which means that after start-up procedures, a separate group of tasks arise and need to be performed by the measurement and control system. Each of the individual task should be designated to the dedicated section of the multi-layered control system [24]. Precise control of each transport air streams is, however, the most crucial task, due to the vertical arrangement of the mill and the counter flow feeding of the fresh material. For any grinding to occur in such a circuit pneumatic transport of the material through the working chamber needs to be ensured. To ensure the desired size reduction of the material grains, mill load level needs to be controlled.

In the discussed circuit, a single pulling fan is the only source of the transport air flow, which is directed into four coupled paths of different capacities (due to different pipes lines). Control system uses dumping flaps to regulate the air flow in each path so the pneumatic transport subsystem is then multi-input and multi-output plant, which realizes different objectives: the main air stream keeps processed material in the working chamber, and can modify the load level of the mill; recycle stream transports oversized material back to the working chamber; additional air stream parameterizes the cut-off grain size of the main classifier and the bypass stream is used to change the total mill's throughput. Such structure causes, however, strong cross-couplings, and any change in one air stream causes changes in another ones. The above problem is solved, by the dedicated algorithms in the supervisory control layer [22].

The structure of the plant can be illustrated by a set of signals that influences plant states. Fig. 7 presents general structure of the circuit as a controlled system. All three transporting air flows: main (F_g), recycle (F_r), and additional (F_d) are enforced by the blower (compare Fig. 3). All of the streams are set by their own flaps. Changes of the position of one flap influence the flow ratio of all streams in the circuit and the output air stream parameters (flow – F_o, temperature – TI_o, and pressure – PI_o). It also influences the solids flow (W_p), load level (LI), and product temperature (TI). Finally, the most important influence concerns the product quality (QI). The circuit reacts similarly on the fresh feed flow changes (F_n), rotating electromagnetic field frequency changes (ω), and volume of the mass flow of the grinding media inserted into the working chamber (F_m). For the control system design purposes, all of the measurable signals were divided into three groups: control signals, disturbances, and system outputs (states). Besides those already described, the signals that are denoted in the structure are: E_w – ratio of volumetric flow of collected air from the cooling fans to taken air volumetric

flow, F_h – volumetric flow of water mist to feed, control voltage, H_g – humidity of the taken air streams, H_d – humidity of air collected from the cooling fans, H_n – fresh feed humidity, T_g, T_r, T_d – main, recycle, and additional air streams temperature, respectively, P_g, P_r, P_d – main, recycle, and additional air streams pressure, respectively, E_f – active power of the inverter.

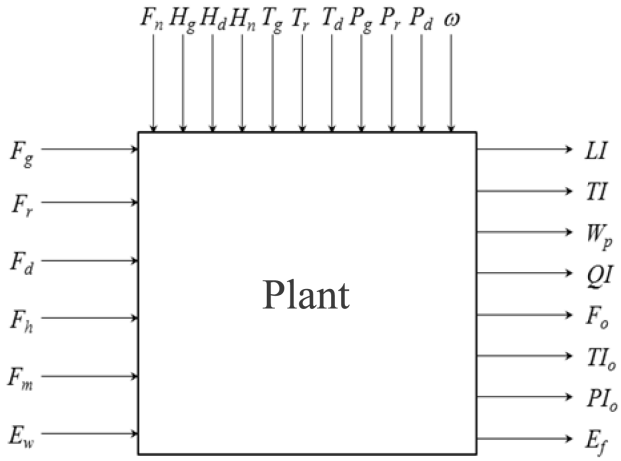

Figure 7: General structure of the plant

From the control point of view dry grinding circuit with EMM is a MIMO plant with complex dynamics that requires hierarchical control system. Since the scope of the paper is dedicated to the direct control of the mill load, tasks designated for each layer will not be discussed. They will, however, be assumed, as described in [24]. Functional structure of the direct control is designed according to the leading variable: fresh material flowrate (the flowrate is determined by the management layer). Fig. 8 presents the functional structure of the mill load control systems. The load level (measured indirectly as LI) is controlled by the transporting air stream directed from the bottom side of the working chamber. The structure is of cascade type. Inner loop (FC) controls the air flow with the set point put out by the outer level control (LC). Leading variable stands for disturbances of the outer loop (slow disturbances), while changes of the air flow (fast disturbances) are regulated by the inner loop, which is the standard motivation for cascade structure application. To improve the inner loop performance, additional pressure compensation (PT) is applied. To improve the outer loop response, additional compensation (ET) of power supply of the electromagnetic mill is applied (slow disturbances as well). Flow controller FC plays the crucial role in the presented structure. Since the pneumatic transport system structure introduces strong cross-couplings, changes of the air flow/pressure in the recycle path change immediately LI, which in turns, involves the reaction of the controller LC and FC. As the

consequence, one obtains changes in air flow/pressure in the main air stream. Dedicated algorithm to counteract such couplings was designed and implemented in the supervisory control layer [24].

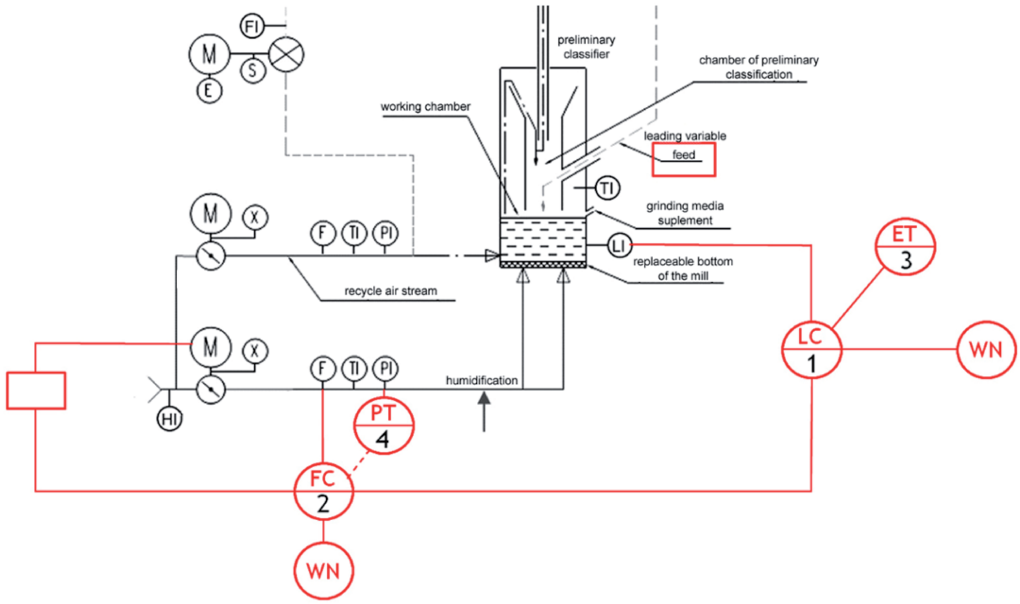

Figure 8: Functional structure of working chamber fulfilment control (measurement points are: F – flow, TI – temperature, PI – pressure, HI – humidity, X – position, LI – level, S – speed, E – voltage, FI – flow of the grains)

3. Model of the controlled plant

Section 2.3 illustrates main coincidences between different variables describing EMM system. The crucial is the control path between main air stream F_g and load level of the chamber LI. Obviously, this path is influenced back by coupling through other part of the control system, especially via supervisory layer. Supervisory controllers determine set points for the flaps controlling F_r and F_d which in terms affect main path. These two streams are also adjusted according to additional states changes namely parameters of output air stream (F_o, TI_o and PI_o), solids output W_p, its quality QI and temperature TI. Over the supervisory layer, the energy optimization task is solved in optimization (operational) level. Optimization algorithm bases on the active power measurement E_f and updates overall production by respective changes of feed F_n, frequency ω flows F_h and F_m and ratio E_w. Humidities H_g, H_d and H_n, pressures P_g, P_r and P_d as well as temperatures T_g, T_r and T_d are treated as the external disturbances. These

disturbances are dumped by compensators (pressures changes), heat recover system which uses cooling fans output (temperatures) and moisture dozing system (humidities).

All the above cross-couplings make the control path between F_g and LI a complex, dynamical, nonlinear and open-loop unstable system. The most important sources of operating point changes in this path are feed F_n, electromagnetic field frequency ω and grinding media load F_m. Other parameters are assumed to follow from the supervisory control layer except F_g which is to be controller by a separate low level controller LC as shown in Fig. 8.

To model the control path $F_g - LI$ artificial recurrent neural network (ARNN) has been applied with three inputs: F_g, F_n and ω and single output LI. Structure of ARNN was chosen as ARMA i.e.:

$$\begin{aligned} LI(i) \;=\; & f(LI(i-1),\ldots,LI(i-n_{LI}),F_g(i-1),\ldots,F_g(i-n_{F_g}),\\ & F_n(i-1),\ldots,F_n(i-n_{F_n}),\omega(i-1),\ldots,\omega(i-n_\omega),F_m). \end{aligned} \tag{2}$$

Parameters n_{LI}, n_{F_g}, n_{F_n} and n_ω were chosen roughly as all equal to 7. This followed from approximative evaluation of the main time constants of the plant which was around 7 [sec] while sampling time was 1 [sec]. F_m was treated as a constant i.e. in a sequel it is expressed as load in [kg], not as a flow.

In order to collect measurement data to learn the network, D200 EMM installation was used. EMM milled limestone with the input cumulative grain size curve shown in Fig. 9 depicted with blue line. After being milled, the product received cumulative grain size curve shown in Fig. 9 in orange (electromagnetic field frequency 50 [Hz]) and green (electromagnetic field frequency 30 [Hz]). The second case was analyzed twice (red line) to become convinced that sieve analysis was performed properly. Experiment which results are shown in Fig. 9 has been conducted for certain parameters as discussed above, however its main goal was to establish air stream F_g which keeps the material inside the chamber not to allow under and overloading. In other words the EMM performed properly in 15 min of time in an open loop state to reach product of the quality shown in Fig. 9.

Main experiments were then performed in open loop for several chosen F_n and ω. In every case, these experiments were followed by initializing trial to establish constant F_g assuring stable load. Example of main experiment result is shown in Fig. 10. The experiments has been repeated as well for changing F_g around the steady value. All data gathered in that manner created input pictures to learn ARNN using back-propagation trough time and Matlab procedures [30].

To learn ARNN data has been divided into two parts as shown in Fig. 11: learning data and testing data. Both responses of ARNN as well as the absolute error shows accurace of the model.

After the model (2) is established, collection of its linear counterpart was easily found by a standard Mean Square method. It is not necessary to make on-

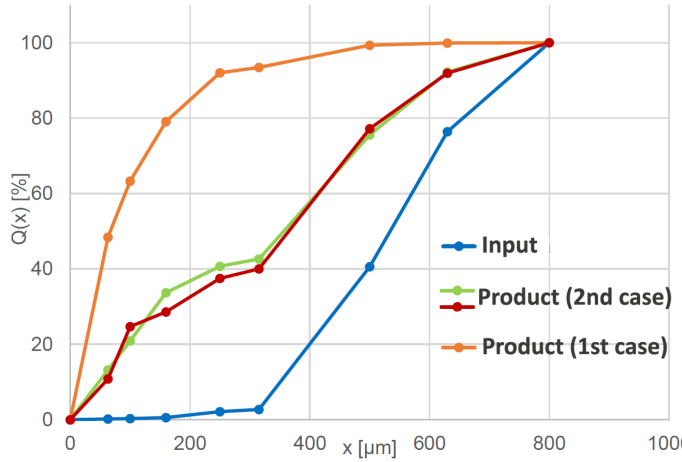

Figure 9: Cumulative grain size of input and product used in the experiments

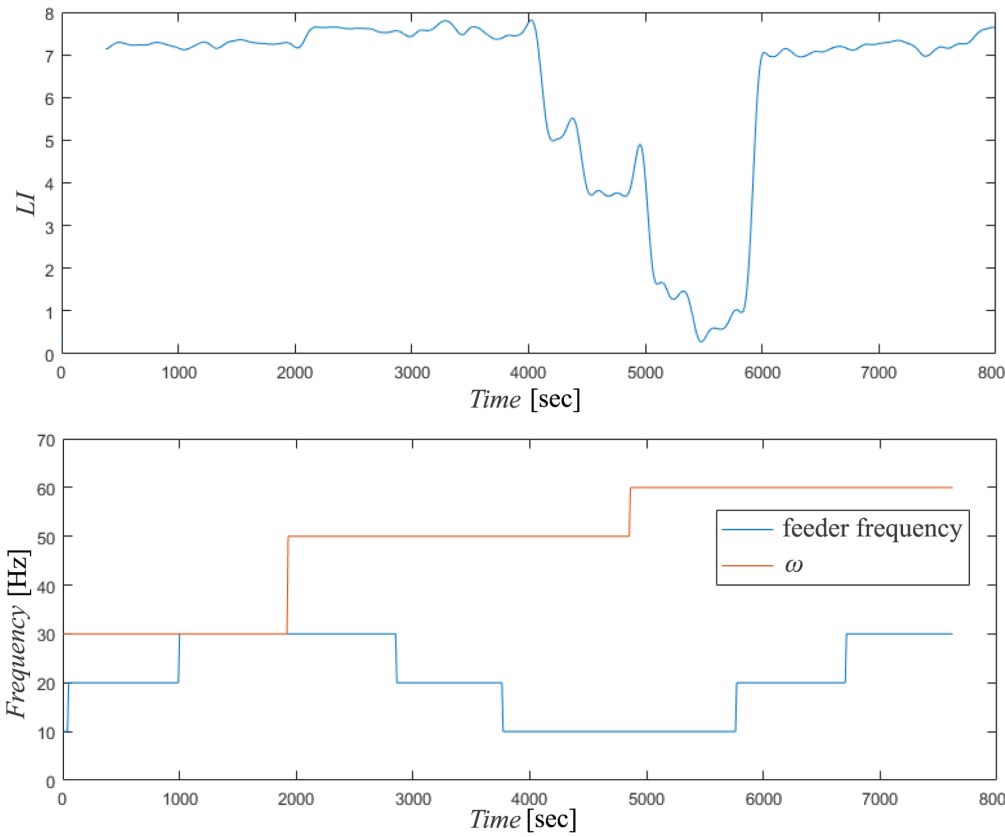

Figure 10: EMM system response to F_n and ω changes for $F_g = 12$ [m/sec]. F_n is expressed in frequency of the screw feeder. LI is expressed in an indirect scale [0–10]

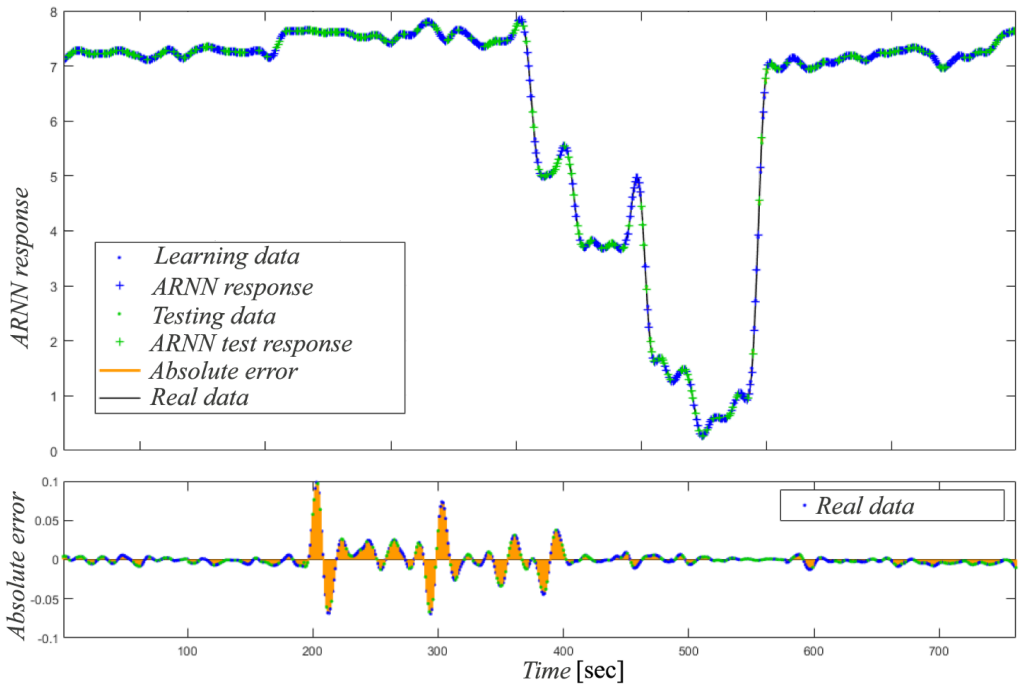

Figure 11: ARNN response and learning error

line linear modeling. What is more, it depends on the user how dense should be division of the operating area into linear subareas i.e. how many linear sub-models need to be created.

4. Predictive control with pole placement

It is shown in [31] that 'classical' predictive linear controllers can not locate the closed-loop system poles in arbitrary places. The complexity of the relation between controller parameters and poles placement is also addressed in [31]. Thus, the 'classical' predictive controllers can not be used directly to solve pole placement problem by tuning their parameters as prediction horizon, control scenario etc. However, the pole placement problem can be solved if the parameterization of the predictive controller is done in a special way as proposed below.

It is shown in [32] that every 'classical' discrete predictive controller can be expressed in the following form

$$\Delta u(i) = u(i) - u(i-1) = \sum_{j=N_1}^{N_2} q_j \epsilon(i+j) \tag{3}$$

where u is the control variable (in the presented case F_g), N_1 and N_2 are minimal and maximal output (in the presented case LI) prediction horizons respectively, $\epsilon(i+j)$ is the prediction of output error defined as a difference between so called reference trajectory $y^r(i+j)$ of the output and so called free response prediction $y^0(i+j)$ of the output

$$\epsilon(i+j) = y^r(i+j) - y^0(i+j). \tag{4}$$

Free response prediction is obtained under assumption that the future control signal is given; for example is constant and equal $u(i-1)$ i.e. $u(i+j) = u(i-1)$, $j = 1, 2, \ldots, N_2-1$. Formula (3) is the solution of the optimization problem:

$$\min_{\Delta u(i+j), j=1,2,\ldots,N_u,\ 1\leqslant N_u\leqslant N_2} \sum_{j=N_1}^{N_2} \left(y^p(i+j) - y^r(i+j)\right)^2 \tag{5}$$

where N_u is the control horizon, $y^p(\cdot)$ is the predicted output (which is the function of the future controls $u(i+j)$) and $y^r(\cdot)$ is the reference trajectory which in general depends on the assumed future set point $w(i+j)$ and in particular can be equal to the future set-point what is assumed in the sequel. If the model of the plant includes influence of stochastic disturbances, then the sum in the equation (5) is taken as a mean (expected) value. This is not a case in this work because pole placement problem does not consider disturbances.

Numbers q_j can now serve as the controller parameters. It is shown below, that these parameters can be chosen in such a way that the closed loop poles can be located in the arbitrary places.

Assume that for the certain parameters of the plant (F_n, ω and F_m), its linear model is expressed with the following discrete transfer function

$$y(i) = z^{-1}\frac{B(z^{-1})}{A(z^{-1})}u(i) \tag{6}$$

where $B(z^{-1}) = b_0 + b_1 z^{-1} + \cdots + n_{nB} z^{-nB}$ and $A(z^{-1}) = 1 + a_1 z^{-1} + \cdots + a_{nB} z^{-nA}$ are coprime polynomials of back-shift operator z^{-1}. Discrete delay time is assumed 1 in the model (6) which is allowed in the predictive control concept and causes soft requirement concerning maximal output prediction horizon N_2 to be greater than the real discrete plant delay time.

For the plant model (6) the controller (3) can be expressed in the general form by means of polynomials $R(z^{-1})$, $S(z^{-1})$ and $T(z^{-1})$

$$R(z^{-1})u(i) = T(z^{-1})w(i) - S(z^{-1})y(i). \tag{7}$$

It is shown in [33] that

$$R = \left(1 - z^{-1}\right)\left(1 + z^{-1}\sum_{j=N_1}^{N_2} q_j V_j^2(z^{-1})\right), \tag{8}$$

$$T = \sum_{j=N_1}^{N_2} q_j \,, \tag{9}$$

$$S = \sum_{j=N_1}^{N_2} q_j G_j(z^{-1}). \tag{10}$$

Polynomials G_j are the solution of diophantine equations

$$1 = \nabla A F_j + z^{-j} G_j, \qquad j = 1, \ldots, N_2 \tag{11}$$

where $\nabla = 1 - z^{-1}$, and polynomials V_j^2 are the result of the following factorization

$$BF_j = V_j^1 + z^{-j} V_j^2, \qquad j = 1, \ldots, N_2. \tag{12}$$

One can easily verify, that the closed-loop transfer function is of the form

$$\frac{y(i)}{u(i)} = z^{-1} \frac{BT}{AR + z^{-1} BS} = z^{-1} \frac{B \sum q_j}{A\nabla + z^{-1} \sum q_j (A \nabla V_j^2 + BG_j)} \,. \tag{13}$$

It follows from (13) that the characteristic equation of the closed–loop system is

$$A_m = \nabla A + z^{-1} \sum_{j=N_1}^{N_2} q_j \left(\nabla A V_j^2 + BG_j \right). \tag{14}$$

Multiplying (11) with B and using (12) one can obtain the following diaphantine equation

$$B = \nabla A V_j^1 + z^{-j} \left(\nabla A V_j^2 + BG_j \right) \tag{15}$$

which shows that

$$\deg \left(\nabla A V_j^2 + BG_j \right) = \max \left(\deg(B) - j, \deg(A) \right). \tag{16}$$

It is now clear from (14) that maximal number of closed–loop poles is equal

$$\max \deg(A_m) = \max \left(\deg(B - N_1 + 1), \deg(A) + 1 \right). \tag{17}$$

Let denote:

$$A_m(z^{-1}) = 1 + m_1 z^{-1} + \cdots + m_{nA_m} \,, \tag{18}$$

$$\boldsymbol{a}^{\nabla} = \left[a_1^{\nabla}, a_2^{\nabla}, \cdots, a_{nA+1}^{\nabla} \right]^T = [a_1 - 1,\ a_2 - a_1,\ \cdots,\ a_{nA} - a_{nA-1},\ -a_{nA}]^T, \tag{19}$$

$$\boldsymbol{r} = [m_1, m_2, \cdots, m_{nA_m}]^T - \boldsymbol{a}^{\nabla}, \tag{20}$$

$$V_j^1(z^{-1}) = v_0^1 + \cdots + v_{j-1}^1 z^{-j+1}. \tag{21}$$

If degree $nA \leqslant nA_m$ then the second vector of the right hand side of (20) should be completed with zeros. Let denote also

$$\Omega_j(z^{-1}) = \nabla A V_j^2 + BG_j = \phi_0^j + \phi_1^j z^{-1} + \cdots + \phi_{nA_m-1}^j z^{-nA_m-1}, \tag{22}$$

$$\Omega = \begin{bmatrix} \phi_0^{N_1} & \phi_0^{N_1+1} & \cdots & \phi_0^{N_2} \\ \phi_1^{N_1} & \phi_1^{N_1+1} & \cdots & \phi_1^{N_2} \\ \vdots & \vdots & \ddots & \vdots \\ \phi_{nA_m-1}^{N_1} & \phi_{nA_m-1}^{N_1+1} & \cdots & \phi_{nA_m-1}^{N_2} \end{bmatrix}. \tag{23}$$

The pole placement problem can be stated as the solution of set of linear equations: given pole placement polynomial (18) find the controller parameters $\boldsymbol{q} = [q_{N_1}, q_{N_1+1}, \cdots, q_{N_2}]^T$ to be the solution of

$$\Omega \boldsymbol{q} = \boldsymbol{r}. \tag{24}$$

The set (24) has the unique solution if rank of matrix Ω is nA_m. The first condition is obvious

$$N_2 - N_1 + 1 \geqslant nA_m\,. \tag{25}$$

Note from (22) that coefficients of polynomial Ω_j are elements of respective columns of matrix Ω. It follows from (15) and (22) that

$$\Omega = \boldsymbol{B} - \boldsymbol{A}\boldsymbol{V}. \tag{26}$$

where

$$\boldsymbol{B} = \begin{bmatrix} b_{N_1} & b_{N_1+1} & \cdots & b_{nB} & 0 & \cdots & 0 \\ b_{N_1+1} & b_{N_1} & \cdots & 0 & 0 & \cdots & 0 \\ \vdots & \vdots & & \vdots & \vdots & & \vdots \\ b_{nB} & 0 & \cdots & 0 & 0 & \cdots & 0 \end{bmatrix}, \tag{27}$$

$$\boldsymbol{A} = \begin{bmatrix} a_1^\nabla & a_2^\nabla & \cdots & a_{nA+1}^\nabla & 0 & \cdots & 0 \\ a_2^\nabla & a_1^\nabla & \cdots & 0 & 0 & \cdots & 0 \\ \vdots & \vdots & & \vdots & \vdots & & \vdots \\ a_{nA+1}^\nabla & 0 & \cdots & 0 & 0 & \cdots & 0 \end{bmatrix}, \tag{28}$$

$$\boldsymbol{V} = \begin{bmatrix} v^1_{N_1-1} & v^1_{N_1} & \cdots & v^1_{N_2-1} \\ 0 & v^1_{N_1-1} & \cdots & v^1_{N_2-2} \\ \vdots & \ddots & & \vdots \\ 0 & \cdots & v^1_{N_1-1} & \cdots\ v^1_{N_2-nA-1} \end{bmatrix}. \tag{29}$$

Matrices $\boldsymbol{B}$, $\boldsymbol{A}$ and $\boldsymbol{V}$ have the same row dimension namely $\max(nB-N_1+1, nA+1)$ thus they should be completed with zero-rows in the bottom respectively. The column dimensions are also the same: $N_2 - N_1 + 1$. It follows from (26) that rows of matrix Ω are composed with subsequent elements of step response of B/A $(v^1_s, v^1_{s+1}, \ldots)$ or their linear combinations. It can be verified that

$$v^1_1 = b_0\,, \tag{30}$$

$$v^1_s = b_s - \sum_{j=1}^{\min(s,nA+1)} a^{\nabla}_r v^1_{s-r}\,, \qquad s = 1, \ldots, nB, \tag{31}$$

$$v^1_s = -\sum_{j=1}^{nA+1} a^{\nabla}_r v^1_{s-r}\,, \qquad s > nB. \tag{32}$$

It is then clear that if polynomials B and A are coprime that Ω is of full rank.

Invertability of the matrix Ω (23) can be also shown using the following relations between its columns. From (15) and (22) it follows that

$$B = \nabla A V^1_j + z^{-j}\Omega_j \tag{33}$$

or

$$B = \nabla A V^1_{j+1} + z^{-j-1}\Omega_{j+1}\,. \tag{34}$$

Subtracting (33) from (34) we obtain

$$0 = z^{-j}\nabla A v^1_j + z^{-j-1}\Omega_{j+1} - z^{-j}\Omega_j \tag{35}$$

which forms series

$$\Omega_{j+1} = z\left(\Omega_j - \nabla A v^1_j\right) \tag{36}$$

with the initial condition

$$\Omega_1 = z\left(B - \nabla A b_0\right). \tag{37}$$

It follows from (36) that

$$\begin{bmatrix} \phi_0^{j+1} \\ \phi_1^{j+1} \\ \vdots \\ \phi_{nA_m-1}^{j+1} \end{bmatrix} = \begin{bmatrix} -a_1^{\nabla} & 1 & & \\ -a_2^{\nabla} & & 1 & \\ \vdots & & & \ddots \\ -a_{nA_m}^{\nabla} & & & 1 \end{bmatrix} \begin{bmatrix} \phi_0^{j} \\ \phi_1^{j} \\ \vdots \\ \phi_{nA_m-1}^{j} \end{bmatrix} \tag{38}$$

or

$$\Omega_{j+1} = \mathbf{\Gamma}\, \Omega_j \,. \tag{39}$$

Now it becomes clear that

$$\mathbf{\Omega} = \left[\Omega_1,\ \mathbf{\Gamma}\Omega_1,\ \mathbf{\Gamma}^2\Omega_1,\ \cdots,\ \mathbf{\Gamma}^{nA_m-1}\Omega_1\right] \tag{40}$$

and we can see that

$$\Omega_{j+1} = \mathbf{\Gamma}\, \Omega_j + \Omega_1 u(j) \tag{41}$$

is the canonical observable form of the system referring to the transfer function

$$K_o\left(z^{-1}\right) = \frac{\Omega_1}{\nabla A} = \frac{z\,(B - \nabla A b_0)}{\nabla A} = z\frac{B}{\nabla A} - z b_0 \,. \tag{42}$$

To summarize above considerations one can formulate the following result.

Theorem 1 *Assume:*

1) *the model of the plant is given by (6) where polynomials B and A are coprime,*
2) *the model is controlled by the predictive algorithm given in the form (3),*
3) *prediction horizons fulfils the condition (25).*

Then:

1) *maximal number of closed-loop system poles which can be placed are given by (17),*
2) *closed-loop pole can be located in arbitrary places by proper choice of the controller parameters $\boldsymbol{q}$ i.e. by solving set of linear equations (26).*

Remark 1 *Maximal number of closed-loop poles does not depend on maximal output prediction horizon N_2. Increasing of the minimal output prediction horizon N_1 may only reduce maximal number of the closed-loop poles.*

Remark 2 *Maximal horizon of the output prediction N_2 should be great enough and minimal horizon of the output prediction N_1 should be small enough to reach condition (25). This condition determinates solvability of the pole placement problem. Positions of the poles may be the same for different combinations of N_1 and N_2 which gives rise a room for robustness considerations.*

Example 1

Consider oscillatory element defined by the following continuous transfer function

$$K(s) = \frac{\omega_n^2}{s^2 + 2\xi\omega_n s + \omega_n^2}, \qquad \omega_n = 0.5, \quad \xi = 0.4 \tag{43}$$

which after discretization with sampling time $T_s = 2$ and zero-order holder element gives discrete counterpart

$$K(z^{-1}) = z^{-1}\frac{0.36 + 0.274z^{-1}}{1 - 0.816z^{-1} + 0.449z^{-2}}. \tag{44}$$

We have

$$\deg_{\max}(A_m) = 3 \tag{45}$$

in this case.

Assume minimum-time response what relates to

$$A_m = \frac{B}{b_0}. \tag{46}$$

If one chose $N_1 = 1$ and $N_2 = 3$ then

$$\boldsymbol{\Omega} = \begin{bmatrix} 0.9278 & 1.2294 & 1.2206 \\ -0.4554 & -1.0120 & -1.1386 \\ 0.1616 & 0.4116 & 0.5520 \end{bmatrix} \tag{47}$$

and

$$\boldsymbol{r} = \begin{bmatrix} 2.5771 & -1.265 & 0.449 \end{bmatrix}. \tag{48}$$

Final controller parameters are

$$\boldsymbol{q} = \begin{bmatrix} 2.7778 & 0 & 0 \end{bmatrix}. \tag{49}$$

The only first element of the vector $\boldsymbol{q}$ is different than zero which is characteristic case of minimum-time response demand. Fig. 12 presents minimum-time response for the unit step change of the set-point. Note, that system responses perfectly in the sampling instants which are pointed in the figure by bullets. Con-

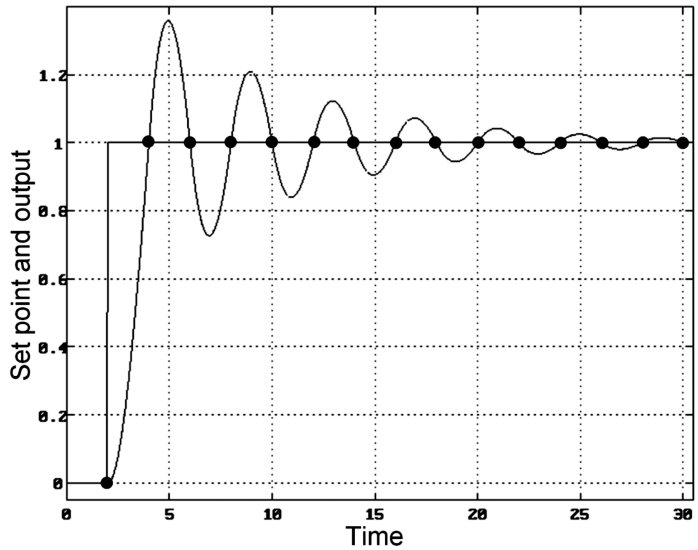

Figure 12: Minimum-time response for the unit step change of the set-point

tinuous counterpart behaves much worse and the control action is also too active, what can be noticed in Fig. 13. These results are well known characteristic of the minimum-time control.

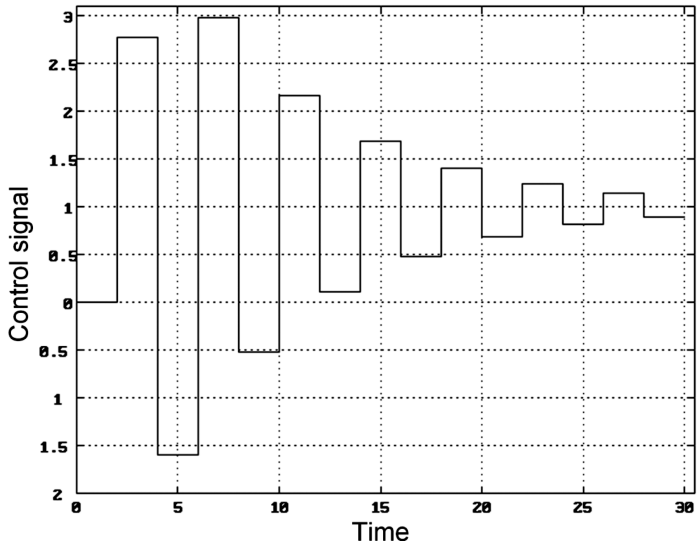

Figure 13: Minimum-time response of the control signal

Example 2

Consider the same case as in Example 1 for dead-beat demand. In this case we have

$$A_m = 1. \tag{50}$$

For the same choice $N_1 = 1$ and $N_2 = 3$ one obtains

$$\boldsymbol{\Omega} = \begin{bmatrix} 0.9278 & 1.2294 & 1.2206 \\ -0.4554 & -1.0120 & -1.1386 \\ 0.1616 & 0.4116 & 0.5520 \end{bmatrix} \tag{51}$$

and

$$\boldsymbol{r} = \begin{bmatrix} 1.816 & -1.265 & 0.449 \end{bmatrix}. \tag{52}$$

Final controller parameters are

$$\boldsymbol{q} = \begin{bmatrix} -0.4294 & -1.8758 & 0.7279 \end{bmatrix}. \tag{53}$$

Figures 14 and 15 presents set-point/output and control signal respectively. Note, that the controller needs three moves of the control signal as the dead-beat does in the case of (45). Continuous counterpart responses much better in the dead-beat case when compare with the minimum-time case.

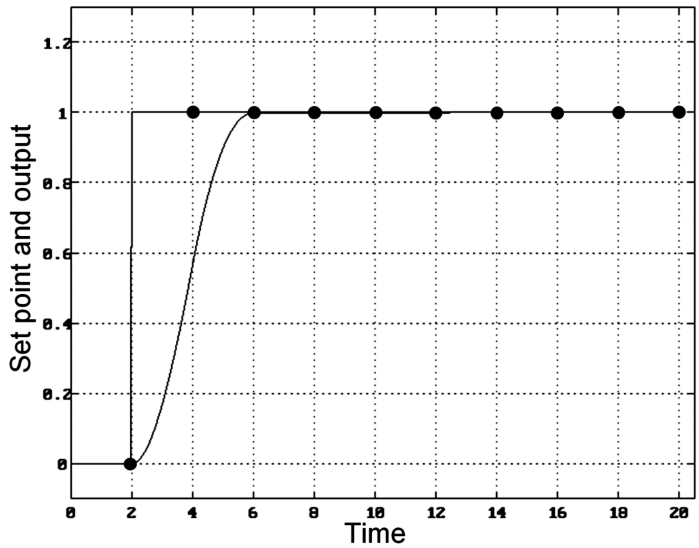

Figure 14: Dead-beat response for the unit step change of the set-point

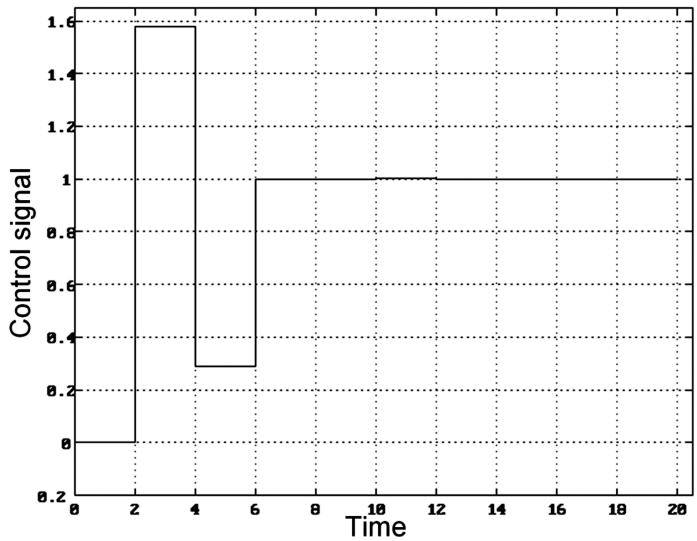

Figure 15: Dead-beat response of the control signal

5. Application to electromagnetic mill system

EMM is equipped with dedicated SCADA and PLC control system that allows for rapid implementation and validations of various control algorithms in every layer of hierarchical control system [24]. As a benchmark, classic PID control was implemented. When the coarse material recycle is closed (oversized grains are directed outside of the circuit), the PID controller LC (Fig. 8) can provide stable LI behaviour, what is presented in [27]. This, however, was reached for a small range of F_n, ω and F_m and number of experiments were needed to tune PID controller properly. If the recycle was switched on (oversized grains were directed again to the mill input), stable response of PID control in the loop F_g–LI was no longer achieved. Small change of any parameter F_n, ω or F_m led to under or overload of the EMM working chamber. Illustration is given in the left part of Fig. 16, where the frequency of screw feeder was changed from 40 to 50 [Hz] at 2000 [sec]. As one can notice EMM system immediately went to the overloaded state although air stream F_g has reacted properly. What needs to be stressed is that the PID controller was not able to stabilize the process with the recycle even for the constant, lower flow of the fresh feed. One can notice fluctuations and drops of the LI signal in the left part of Fig. 16 before the feeder frequency was changed in 2000 [sec]. Presented case was chosen on purpose because it shows the EMM system working close to the "fully-loaded" operating point what is desired from technological and economical point of view. Any sudden drop in the LI signal quickly lead to the "over-loaded" state. Experiment was stopped due to complete overload of the EMM.

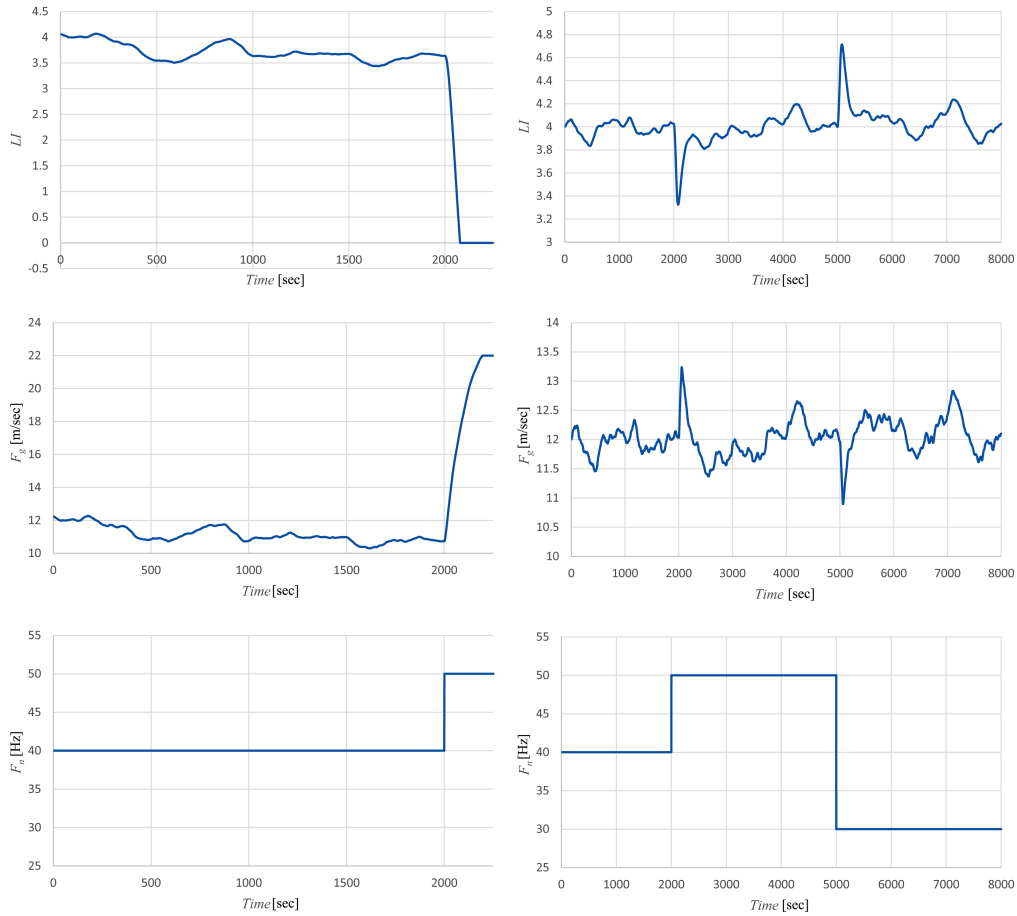

Figure 16: Instability of PID control (left part), and stable response of predictive control (right part)

Right part of the Fig. 16 presents example of the control system response after implementation of the predictive control algorithm with pole placement in the dedicated SCADA and PLC modules. Right bottom part of Fig. 16 presents excitation used in the experiment: frequency of the screw feeder was changed from 40 [Hz] to 50 [Hz] at 2000 [sec] as in the experiment with PID controller and then went back down to 30 [Hz] at 5000 [sec]. Such changes serve as a huge disturbance in the system significantly changing the operating point. Initial conditions for this experiment were similar to the one with the PID controller i.e. EMM system was also almost fully loaded according to the LI signal indication (compare Fig. 6). Predictive controller (3) was used with $N1 = 1$ and $N2 = 12$. Since n_B and n_A was not less than 4 in model (6), the polynomial A_m degree has

been chosen just equal 4. The closed-loop system poles were chosen as follows: 0.98, 0.96, 0.96 and 0.965 i.e.

$$A_m = 1 - 3.865z^{-1} + 5.6017z^{-2} - 3.6083z^{-3} + 0.8716z^{-4}. \tag{54}$$

Linear model of the plant has been changed three times during operation shown in the right part of Fig. 12 which corresponds to three steady values of F_n (40, 50 and 30 [Hz] of the screw feeder frequency). Despite the degrees n_B and n_A were different in these three models, the system could keep the same poles of the closed loop in every case. Indeed, it can be seen in the right part of Fig. 16 that the response on F_n step changes are more or less the same, the only directions are opposite. Obviously, keeping maximal predictive horizon N_2 long enough (12 in the presented example) makes the system robust against particular change of linear model order while operating point changes.

It is worth to emphasise a slow drift of LI signal in the first 2000 seconds of experiment in PID case when compared with proposed algorithm, what is shown in Fig. 17. Initial value of the screw feeder frequency was 30 up to 2000 [sec].

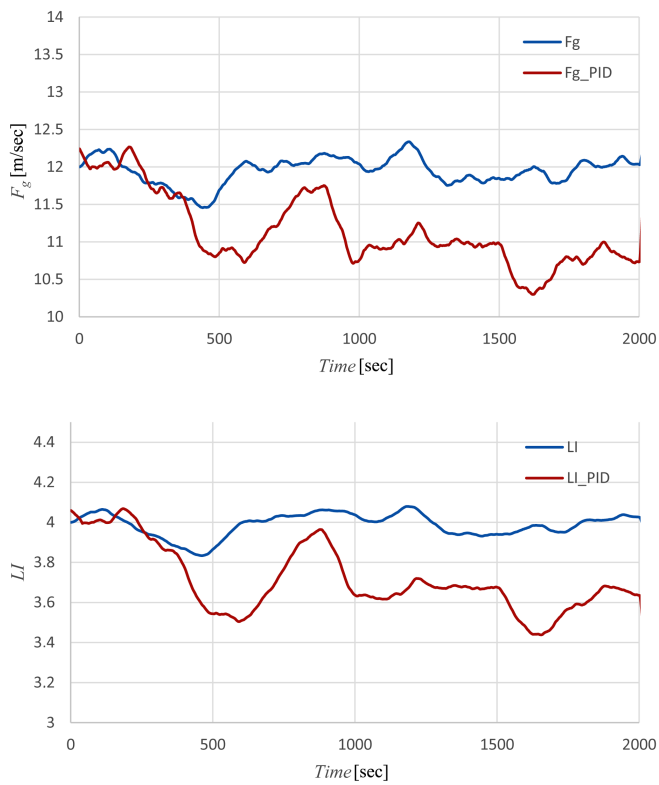

Figure 17: Comparison of PID controller response (drift) with stable resposponse of predictive control

Drift can be observed in PID case, while predictive controller keeps average value of LI close to set-point equal 4.

Similar responses were obtained if other excitations occurred i.e. ω or F_m. It is important to note that all other parts of the control system were active during the experiments i.e. supervisory control and optimization layer.

6. Conclusion

Predictive control with pole placement may be treated as the adaptive gain scheduling control. Nonlinear ARNN model is parameterized with F_n, ω and F_m, thus these three variables serve as additional measurements that take part in the "scheduling" of the control gain changes. Scheduling in this case means, however, recalcuation of the controller parameters using linear approximation of nonlinear ARNN model in the vicinity of the actual operating point. Fortunately, all calculations may be performed off-line and simple look-up table technique can be applied. Such approach simplified the calculations and actions of the supervisory layer implemented in the dedicated SCADA module as well as the actions of the direct control implemented in the PLC.

The prospective work will concern poles location choice. For certain operating points the poles location becomes difficult due to contradictory demands of related required speed of the system response. Additional challenge imposes indirect measurement of LI which slows down the system response. As it has been stated in sec. 3, some of the disturbances were uncompensated. After compensation is done, dynamical complexity of the control path F_g–LI become even greater which serves as yet another area of the prospective work.

ARNN fulfilled the task of plant modeling. However, every experiment that allowed data acquisition for the identification purposes needed to be followed by the proper choice of F_g which assured stable behaviour of the system in the open loop. It was difficult, time consuming research requiring multiple repetitions. The improvement may be found in an identification while the loop is closed by roughly tuned predictive controller. This would be the first step to develop adaptive version of the presented algorithm.

References

[1] C. Shang: *Dynamic Modeling of Complex Industrial Processes: Data-driven Methods and Application Research*, Springer Theses. 2018.

[2] M.J. Grimble: *Industrial Control System Design*, Wiley, 2001.

[3] M.C. Fuerstenau and K.N. Han (Eds.): *Principles of Mineral Processing*, SME, 2003.

[4] T.J. Napier-Munn, S. Morrell, and R.D. Morrison: *Mineral Comminution Circuits: Their Operation and Optimization*, Julius Kruttschnitt Mineral Research Centre, University of Queensland. 1996.

[5] T. Tumidajski, E. Kasinska-Pilut, T. Gawenda, Z. Naziemiec and R. Pilut: Investigation of grinding process energy consumption and grindability of lithologic components of Polish copper ores, *Miner. Resour. Manag.*, **26** (2010), 61–72.

[6] D. Hodouin: Methods for automatic control, observation, and optimization in mineral processing plants, *Journal of Process Control*, **21** (2011), 211–225.

[7] J. Kolacz and K.L Sandvik: Ultrafine grinding in an air-swept ball mill circuit, *Int. J. Miner. Process.*, **44 – 45** (1996), 361–371.

[8] J. Richalet, A. Rault, J.L. Testud and J. Papon: Model algorithmic control of industrial processes, *IFAC Proceedings Volumes*, **10**(16) (1977), 103–120.

[9] C.R. Cutler and B.L. Ramaker: Dynamic matrix control – a computer control algorithm, *Proceedings Joint Automatic Control Conference*, San Francisco, CA, USA, (1980).

[10] D.W. Clarke, C. Mohtadi and P.S. Tuffs: Generalized predictive control. Part I: The basic algorithm. *Automatica*, **23**(2) (1987), 137–148. Generalized predictive control. Part II: Extensions and interpretations, *Automatica*, **23**(2) (1987), 149–160.

[11] D.Q. Mayne and H. Michalska: Receding horizon control of nonlinear systems, *IEEE Transactions on Automatic Control*, **35** (1990), 814–824.

[12] R. Bitmead, M. Gevers and V. Wertz: *Adaptive Optimal Control the Thinking Man's GPC*, Prentice-Hall, Englewood Cliffs, NJ, 1990.

[13] Z. Ogonowski: *Discrete Predictive Control with the use of Weighting Function*, PhD dissertation. Silesian Unversity of Technology, 1987 (in Polish).

[14] D. Bismor, K. Jablonski, T. Grychowski and S. Nas: Hardware-In-the-Loop Simulations of a GPC-Based Controller in Different Types of Buildings Using Node-RED, *Advanced, Contemporary Control*, 1018–1029, Springer International Publishing, 2020. ISBN: 978-3-030-50935-4, doi: 10.1007/978-3-030-50936-1.

[15] Y. Wang and S. Boyd: Fast model predictive control using online optimization, *IEEE Transactions on Control Systems Technology*, **18**(2), (2010), 267–278.

[16] R. Nebeluk and P. Marusak: Efficient MPC algorithms with variable trajectories of parameters weighting predicted control errors, *Archives of Control Sciences*, **30**(2), (2020), 325–363.

[17] A. Bemporad, M. Morari, V. Dua and E. Pistikopoulos:The explicit linear quadratic regulator for constrained systems, *Automatica*, **38**(1), (2002), 3–20.

[18] M. Lawrynczuk: Computationally Efficient Model Predictive Control Algorithms: a Neural Network Approach, Studies in Systems, Decision and Control, **3** Springer, Cham, 2014.

[19] M. Lawrynczuk: Nonlinear state-space predictive control with on-line linearisation and state estimation, *International Journal of Applied Mathematics and Computer Science*, **25**(4), (2015), 833–847.

[20] K. Slawinski, M. Gandor, K. Knas, B. Balt and W. Nowak Electromagnetic mill and its application for coal drying process, *Rynek Energii*, **1** (2014), 140–150.

[21] M. Pawelczyk, Z. Ogonowski, S. Ogonowski, D. Foszcz, D. Saramak, T. Gawenda and D. Krawczykowski: Method for Dry Grinding in Electromagnetic Mill. Patent PL413041, 06.07.2015.

[22] S. Ogonowski, Z. Ogonowski and M. Pawelczyk: Model of the air stream ratio for an electromagnetic mill control system. *In Proceedings of the 21st International Conference on Methods and Models in Automation and Robotics (MMAR 2016)*, Miedzyzdroje, Poland, (2016), 901–906. doi: 10.1109/MMAR.2016.7575257.

[23] M. Wolosiewicz-Glab, S. Ogonowski, D. Foszcz and T. Gawenda: Assessment of classification with variable air flow for inertial classifier in dry grinding circuit with electromagnetic mill using partition curves, *Physicochem. Probl. Miner. Process.*, **54** (2018), 440–447, doi: 10.5277/ppmp1867.

[24] S. Ogonowski, Z. Ogonowski and M. Pawelczyk: Multi-objective and multi-rate control of the grinding and classification circuit with electromagnetic mill. *Appl. Sci.*, **8** (2018), 506, doi: 10.3390/app8040506.

[25] A. Casali, G. Gonzalez, F. Torres, G. Vallebuona, L. Castelli and P. Gimenez: Particle size distribution soft-sensor for a grinding circuit, *Powder Technology*, **99** (1998), 15–21. doi: 10.1016/S0032-5910(98)00084-9.

[26] A.K. Pani and H.K. Mohanta: Soft sensing of particle size in a grinding process: Application of support vector regression, fuzzy inference and adaptive neuro fuzzy inference techniques for online monitoring of cement fineness. *Powder Technology*, **264** (2014), 484–497, doi: 10.1016/j.powtec.2014.05.051.

[27] S. Ogonowski, Z. Ogonowski, M. Swierzy and M. Pawelczyk: Control system of electromagnetic mill load, *25th International Conference on Systems Engineering (ICSEng)*, Las Vegas, NV, USA, (2017), 69–76, doi: 10.1109/ICSEng.2017.23.

[28] M. Pawelczyk, Z. Ogonowski and S. Ogonowski: Control of electromagnetic mill working chamber load in pneumatic transport circuit. Polish Patent Application P.421160, 15.03.2017.

[29] H.J. Nussbaumer: *Fast Fourier Transform and Convolution Algorithms*, Springer Verlag, New York, 1982.

[30] J. Moscinski and Z. Ogonowski (Ed.): *Advanced Control with Matlab and Simulink*, Prentice Hall Inc. 1995.

[31] Z. Ogonowski: Application of predictive control to nonlinear MIMO systems, *IFAC Work-shop on New Trends in Design of Control Systems*, Smolenice, Slovak Republic (1994).

[32] R.J. Evans, A. Cantoni and K.J. Ahmed: Envelope-constrained filter with uncertain input, *Circuits Sysr. Signal Processing*, **2**(2), (1983), 131–154.

[33] A. Niederlinski, J. Moscinski and Z. Ogonowski: *Adaptive Control*, PWN, Warsaw, 1995 (in Polish).